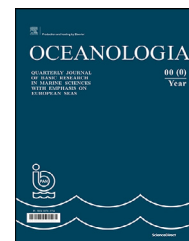


Available online at www.sciencedirect.com

ScienceDirect

journal homepage: www.journals.elsevier.com/oceanologia

ORIGINAL RESEARCH ARTICLE

Rip currents in the non-tidal surf zone with sandbars: numerical analysis versus field measurements

Aleksandra Dudkowska^{a,*}, Aleksandra Boruń^a, Jakub Malicki^b,
Jan Schönhofer^b, Gabriela Gic-Grusza^a

^aUniversity of Gdańsk, Institute of Oceanography, Gdynia, Poland

^bInstitute of Hydro-Engineering, Polish Academy of Sciences, Gdańsk, Poland

Received 14 August 2019; accepted 7 February 2020

Available online 22 February 2020

KEYWORDS

Rip current;
Coastal zone;
Coastal flows;
Wind-wave conditions

Summary Rip currents, which are local seaward-directed jets with their mean velocity exceeding 0.5 m/s, have been a subject of many studies since the 1940s. They are an important part of the nearshore current system and in specific hydro- and geomorphological conditions can cause changes in the local bathymetry. Thus, a detailed analysis of the characteristics of this phenomenon is crucial both to public safety and hydroengineering. The main purpose of this research is to determine the wave conditions of a multi-bar non-tidal coastal zone environment in which rip currents can occur. In this study, we focus on a multi-bar non-tidal coastal zone environment located in the Southern Baltic Sea, where rip current driving forces are mostly reduced to the wind and wind-induced waves. This is one of very few comprehensive approaches to exploring the possibility of rip currents occurrence in such environmental conditions. During two field expeditions, there were carried out in situ measurements exploiting two GPS drifters. The results indicate the formation of irregular non-longshore flows (related to rip currents) in the studied area. To answer the question under what conditions the formation of rip currents takes place, an extended modelling experiment was performed. Deep-water wave conditions typical of the studied area were chosen due to buoy measurements. The total of 589 combinations of the significant wave height, the mean period and wave direction values were examined

* Corresponding author at: University of Gdańsk, Institute of Oceanography, Piłsudskiego 46, 81–378 Gdynia, Poland.

E-mail address: aleksandra.dudkowska@ug.edu.pl (A. Dudkowska).

Peer review under the responsibility of the Institute of Oceanology of the Polish Academy of Sciences.



Production and hosting by Elsevier

<https://doi.org/10.1016/j.oceano.2020.02.001>

0078-3234/© 2020 Institute of Oceanology of Polish Academy of Sciences. Production and hosting by Elsevier B.V. This is an open access article under the CC BY-NC-ND license (<http://creativecommons.org/licenses/by-nc-nd/4.0/>).

as test cases. The coastal flow in the area and tracks of virtual drifters were simulated by XBeach numerical model for all test cases. As a result, 589 nearshore currents fields were generated and two scenarios were indicated: a regular circulation (dominated by the longshore current) which is typical of this area (547 cases), and flows with rip current features (42 cases). This reflects the results of the field measurements carried out. It can be concluded that the wave direction is a dominating factor in the formation of rip currents. Namely the flows of this type may occur in the area of interest when the direction of a deep water wave is almost perpendicular to the shore. Such situations occur rarely. They cover about 7% of the days of the year. Thus, rip currents do not appear to be a significant factor in the reconstruction of the sea bottom in the studied area.

© 2020 Institute of Oceanology of Polish Academy of Sciences. Production and hosting by Elsevier B.V. This is an open access article under the CC BY-NC-ND license (<http://creativecommons.org/licenses/by-nc-nd/4.0/>).

1. Introduction

Coastal zone morphodynamics of the non-tidal inner sea is affected by complex three-dimensional flows of water, generated mostly by waves. Coastal sediment transport is primarily caused by the so-called longshore current, which is the dominating part of the current system. Cross-shore sediment transport is normally induced by the undertow. Such hydrodynamics is directly related to multi-bar seabed forms. Apart from these typical flows, some specific hydro- and geomorphological conditions occasionally form seaward-directed quasi-steady jets. These so-called rip currents originate within the surf zone and broaden outside the breaking region. The physical driving mechanisms crucial to the generation of rip currents is alongshore variability in breaking wave energy dissipation (Pitman et al., 2016). There have been identified a number of different causes of this variability, which is linked to the different types of rip currents along beaches (Castelle et al., 2016; Kirby, 2017). According to the traditional approach, a typical hydrodynamic background is the convergence of the two opposite-directed longshore flows, i.e. feeder currents, resulting from the longshore variability of the wave-induced set-up, caused by the gradients of radiation stresses (Longuet-Higgins and Stewart, 1964). The emerging offshore flow is called a rip current. It may result in a recess in the bar and if the phenomenon lasts long enough, a channel is formed. This so-called energy window is a potential place for the emergence of the next rip current, which deepens the channel. As a result of this positive feedback between waves, currents and morphology (Garnier et al., 2008), a local disturbance of the bathymetry may initiate the generation of a rip current (Sabet and Barani, 2011). This type of rips – channel rip currents – are the most documented in barred surf zones (Castelle et al., 2016). However, complex lito- and hydrodynamics can provide a number of mechanisms driving rip currents, which act simultaneously. Resulting rips are temporary in space and time. Another theoretical approach was applied by (Bruneau et al., 2011) and is based on interpretation of surf zone flows on the basis of their vorticity proposed by (Peregrine, 1998). The authors derived a conservation equation of the vertical vorticity of the mean wave-driven currents, which provides information on rip current circulations that was difficult to interpret using the traditional radiation stress approach.

One of the most commonly used approaches when observing rip currents in the environment are Lagrangian measurements combined with other methods. (Johnson and Pattiaratchi, 2004) recorded transient rip currents, with perpendicular incident swell waves, while carrying out Eulerian and Lagrangian measurements of the nearshore circulation on a longshore uniform beach in Western Australia. (Castelle et al., 2014; Floc'h et al., 2018) used human drifter data (human operators that drifted with the currents, each equipped with a GPS) and video imagery technique. The method based on color processing of video images enables researchers to detect the presence of rip currents via a change of turbidity. They detected numerous rips along the coast of the Gulf of Guinea, exposed to high-energy waves generating strong nearshore currents.

In this paper we focus on the Southern Baltic coastal zone rip currents, which are still a lesser-known phenomenon. The first traces of their occurrence were discovered in 1970 by Rudowski (Rudowski, 1970), who noticed seabed ripple marks arranged in a characteristic pattern. In the following years Furmanczyk (Furmańczyk, 1994) noted some distinctive breaks in bars in the aerial and satellite photographs of the Pomeranian Bay, which he explained by means of rip currents. Also, Pruszek (Pruszek et al., 2008) describes the periodic mega-cusps occurring on the Southern Baltic coast after a storm. Observations conducted by Schönhofer (Schönhofer, 2014), which are regarded as a pioneering study related to the scope of this work, confirmed the occurrence of rip currents in south Baltic shore. During field surveys in Coastal Research Station (CRS) Lubiato, he registered several cases of flow with some features characteristic of rip currents. The measurements with the use of two GPS drifters were carried out during approximately 20 days in years 2011–2013. The rip-current type flows were registered during 4 surveys in which there were similar wave conditions, i.e. the wave was moving from NNW to NNE, and the wave steepness was about 0.025.

These observations confirm the theory that rip currents on the dissipative coasts are induced by long waves, characterized by a small steepness (a small wave height compared to its length), and they can reach the coast without breaking over the bars. Thus, waves bring energy to the coast, the way it can be observed at the steep coasts. A favourable condition is a swell when short-wind waves disappear and long waves occur. Long waves undergo a stronger refraction,

so regardless of the direction in which they approach the shore in the deep water, they are almost perpendicular to the shore in the shallow water (Schönhofer, 2014).

Assessing the risk of rip-current occurrence is important for the scientific as well as the beach-safety purpose. A better understanding of this phenomenon is essential for the development of a predictive system working in an operational mode. Such warning systems, based on a series of measurements of the coastal zone currents were created, among others, for the south-east coast of the USA (MacMahan et al., 2006; 2005), as well as for the Dutch coast (Sembiring et al., 2014). In order to forecast, among other parameters, the possibility of rip current occurrence in the area of the Southern Baltic in selected locations, a pilot predictive system based on XBeach model in 1D mode was implemented (Furmańczyk et al., 2014). This indicator was based on the assumption that rip currents appear when waves break over submerged longshore bars near the shoreline (Short and Aagaard, 1993).

However, to develop an effective system of a rip current forecast for the Baltic, it is necessary to determine the environmental conditions that can be conducive to this phenomenon. Both in situ observations and the theory of rip currents formation suggest that: (1) the wave direction – perpendicular to the shore and (2) the wave steepness – relatively small, are conditions favourable for the generation of rip currents in the studied area. However, a small amount of observational data is insufficient to confirm these hypotheses. Detailed field measurements are difficult, because rip currents are very unpredictable. As it is problematic to observe in situ the nearshore flow in a wide range of hydro- and morphological conditions, the modelling approach seems to be the only way to investigate the phenomenon comprehensively.

Various approaches to the rip currents modelling have been taken. Generally accepted methods applied in simplified basins with regular bathymetry include 3D hydrostatic or Boussinesq modelling. In contrast, a number of modelling studies of coastal zone currents in the real environments with complex topography are based on spectral 2D models. A likely explanation is a compromise between accuracy and the computational cost. An example is the study carried out by (Johnson and Pattiaratchi, 2006) in which a spatially variable wave field was simulated with the model *Funwave* based on the fully nonlinear Boussinesq equations. For a set of different beach slopes and wave spectra variable wave-averaged currents were generated and sometimes transient rip currents were formed. On the other hand (Xie, 2012) showed, that his coupled wave–current 3D model can effectively describe the rip current 3D structures under irregular bathymetry. Apart from successful modelling attempts in artificial basins with a simplified bathymetry, modelling was carried out in the real locations with a complex sea bottom topography. Among others, interesting research was conducted for the region of Egmond aan Zee in The Netherlands, a typical area of the Dutch coast barred coastline. This location is appropriate for studying rip currents in the environment with a strong horizontal tide. A notable example is research conducted by (Winter et al., 2014) based both on (1) in-situ measurements in the surf zone with drifter instruments and (2) modelling with the use of a 2DH numerical model XBeach. Another interesting study in this

location was carried out by (Sembiring et al., 2014) in which an operational model for the nearshore zone provides the prediction of the location, strength and timing of rip currents. The study used a novel approach in which the input to an XBeach model was the video-derived bathymetry.

The aim of this study is to determine whether, under given wave conditions, the generation of rip currents in the multi-bar coastal zone of the Southern Baltic Sea is possible. Our research is the first attempt of a systematic approach to this topic, i.e. it includes all possible wave conditions in the given region. To achieve this, the following assumption was made: the factor responsible for the rip current initiation is the break in the bar – preceding non-linear complex processes leading to the formation of the rip channel are not considered. Thus, we address the research question: What is the minimal frequency of the rip currents occurrence, and whether rip currents are important factors in the processes of seabed and beach rebuilding in the multi-bar coastal zone of the non-tidal inner sea.

Both measurement data and modelling results was used in the presented study. Wave buoy measurements together with other multi-aspect field investigations carried out for many years by the Institute of Hydro-Engineering of the Polish Academy of Sciences (IBW) provided huge amount of data and observations of the coastal zone, which are the background of this study. Long-term buoy measurements provided the basis for determining deep-water wave conditions typical of the studied area. 589 modelling scenarios covers all wave conditions likely in the studied region. Lagrangian field measurements with the use of free GPS drifters were performed to estimate the local coastal flows. During these measurements a flow of rip current type was recorded, similar to this described in the work (Schönhofer, 2014). This registered flow served as an example of the phenomenon in the studied area and its features were then used to verify the results of numerical modeling. Numerical simulations are the optimal way to analyze flows for a wide range of wave conditions. The coastal flow in the area and tracks of virtual drifters were simulated by the numerical model XBeach (Roelvink et al., 2010). The set-up of the model was calibrated firstly by comparison of the modelled wave parameters to the results of SWAN model (Booij et al., 1996), which was validated in previous studies (Reda and Papińska, 2002). Secondly, the tracks of virtual tracers and their velocities were compared to the in situ measured flows. After the model calibration, a nearshore wave and currents fields were simulated for all 589 test cases.

In this work only bathymetry controlled rip currents were simulated. This is the best-documented driving mechanism in barred coastal zones, however, numerous possible scenarios of the rip current initiation are possible. The presented results indicate that the phenomenon of rip currents in the studied area is rare and that it is not a significant factor in the morphodynamic processes.

2. Study area

The study area is located in the Southern Baltic, within Polish Marine Areas (see Fig. 1), adjacent to the coastline in the vicinity of Lubiatowo village, where The Coastal Research Station (CRS) – a field laboratory of the Institute of Hydro-

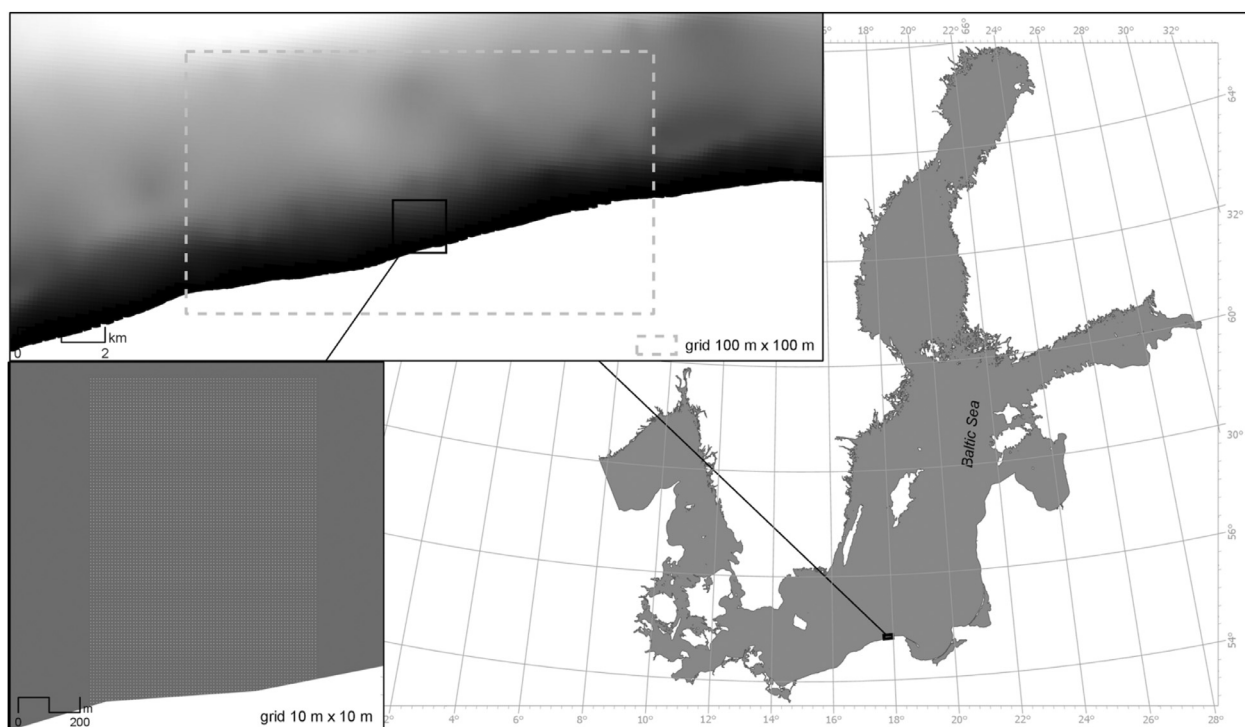


Figure 1 Area of interest and the computational meshes used in numerical modelling: SWAN external grid 100 m × 100 m; SWAN (internal) and XBeach grid 10 m × 10 m.

Engineering of the Polish Academy of Sciences (IBW PAN) – is situated. This area is well-researched and is a representative sample of the Southern Baltic coast. It is characterized by a rather stable shore, with a mild erosive tendency observed over the last years. The slope of the sea bottom is approximately 1.5% (with a value of up to 4% locally, near the shoreline). Along the section of the shore, there can typically be five offshore bars: four permanent and one occurring temporarily, in the distances from the shoreline of approximately: 100–120 m, 200 m, 400–450 m, 650–850 m. As it is difficult to perform bathymetric measurements during strong waves, typical bathymetry for Lubiatowo area was used for modelling, Fig. 2. Principal water depth is about 8 m at 1 km from the shoreline and it increases to about 15–17 m at 2 km and to 25 m at 9 km. The bottom profile is relatively uniform along the coastline (Ostrowski et al., 2016).

3. Material and methods

Nearshore flow measurements

In order to examine nearshore flow in situ, two field surveys in CRS Lubiatowo under different deep water wave con-

Table 2 The technical specification of drifters.

	ballast [kg]	displacement [dm ³]	height [m]	immersion [m]
A	2	2.5	0.8	0.2
B	7	7.5	1.0	0.2

ditions were carried out: 14.01.2016 the significant wave height H_s was about 1.8 m and the wave steepness ξ was about 0.02, while 15.04.2016 H_s was about 0.5 m and ξ was about 0.01. Other weather and sea conditions during expeditions are summarized in Table 1.

Lagrangian field measurements were carried out with the use of free GPS drifters. Both the preparation of the GPS drifters and the organization of the field expeditions were carried out by IBW. Two drifters (marked A and B) with GPS modules with internal memory attached were used. The drifters were released near the coastline, their positions were recorded and the coastal flows were estimated. For technical details see Fig. 3 and Table 2.

The drifters are built of buoy and ballast that stabilized movement on the water surface. Additionally there was

Table 1 Environmental conditions during field expeditions: wave data from a wave buoy located about 1.5 NM offshore (54°50.360'N, 17°50.301'E), the water depth in the buoy location is about 18 m. The experiments were performed within less than one hour the period in which wind and wave conditions could be considered stable.

	H_s [m]	T_p [s]	ξ	Θ_{wave} [°]	T_{water} [°C]	T_{air} [°C]
14.01.2016	1.8	7.7	0.02	11	0.5	4.3
15.04.2016	0.5	6.5	0.01	5	7.0	13.0

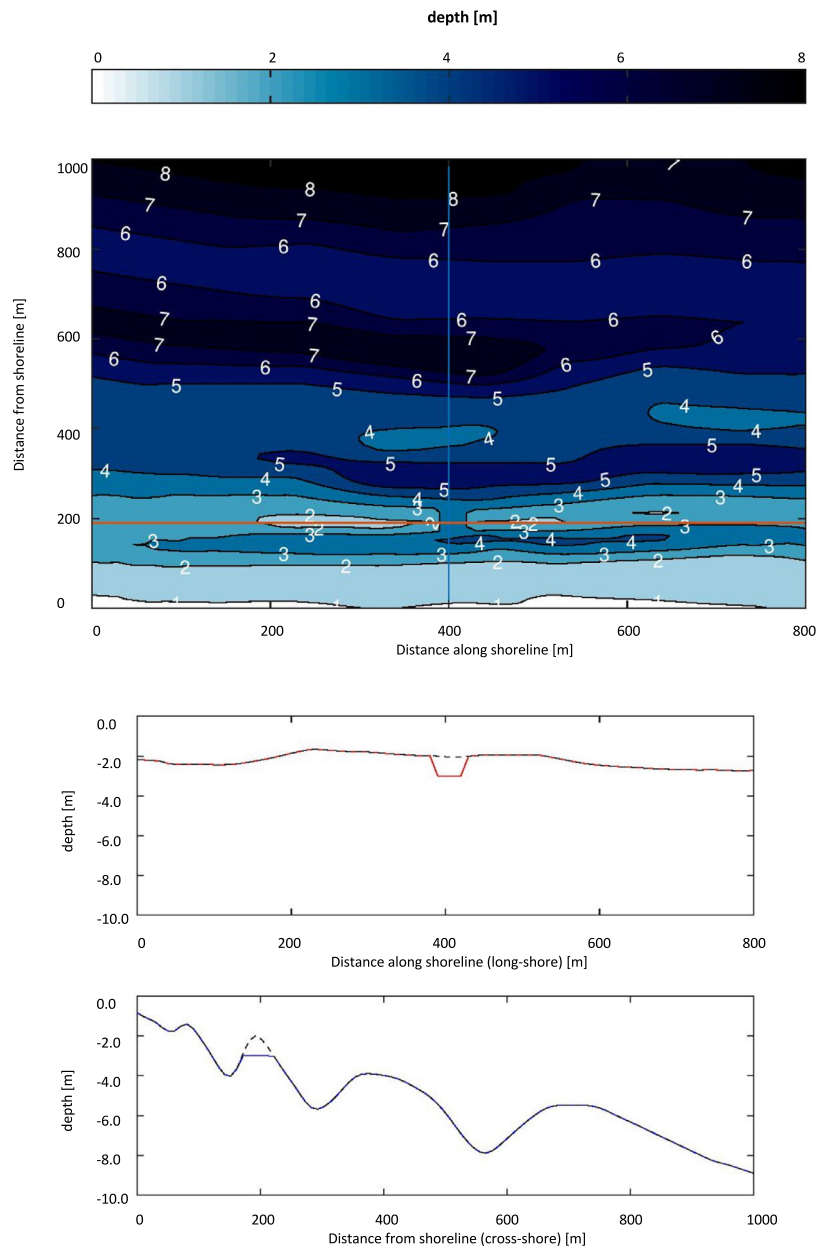


Figure 2 Top panel: bathymetry of CRS in Lubiatowo, bottom panel: long-shore and cross-shore bottom profiles in the area of rip channel, the black dotted lines are profiles without gap in the bar.

attached a drogue submerged about 0.7 m below the surface of the water, and at shallow depths it floated near the bottom. The underwater drogue ensured the drifter followed the movements of the water and was carried by bottom currents as well as the surface ones. Therefore, it can be assumed that the drifters movement represent a depth-averaged water current. The GPS drifters were released behind the first stable bar, at a distance of 100–150 m from the shoreline, at a depth of about 1.5 m. Typically, they floated along the shore and their positions were recorded continuously and read after removing the device from the water. After some time, they returned to the beach, see Fig. 4, were thrown again and continued the route along the shore. Aerial photo (Head Office of Geodesy and Cartography) is demonstrative and was done

prior to the measurements, so in some cases the drifters' trajectories end at the beach, which actually didn't happen.

This method was used to measure approximately 1700 m of the beach territory. During the first expedition the following data were recorded: (1) six throws of drifter A, and four throws of drifter B; (2) during the second expedition three throws of drifter A.

Determining deep water wave conditions typical of the studied area

Deepwater waves conditions were determined based on measured by wave buoy Datawell BV DWR-7 Mk. III in 2013–2018 parameters. The buoy was anchored in the nearshore

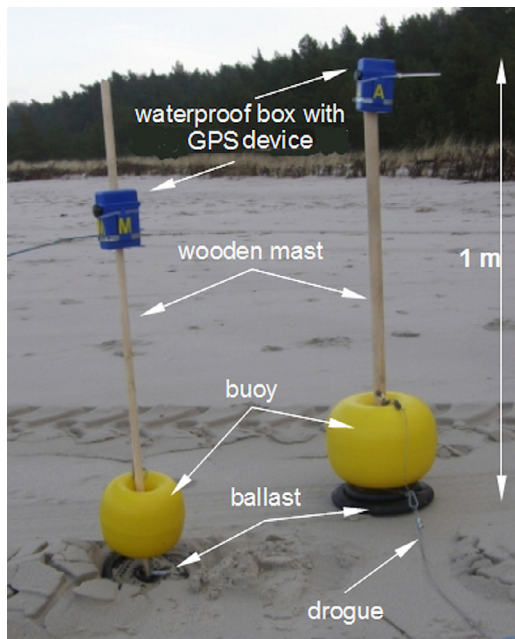


Figure 3 Drifters used for in situ measurements: A (smaller one) and B (bigger one).

beach in Lubiatowo village in the point: 54°50.360'N, 17°50.301'E at a distance of about 1.5 NM. The water depth of the anchored point was about 18 m. The buoy measured such parameters as: significant wave height, wave

period, wave direction, water temperature at prevailing 10 minutes interval. The buoy does not record very short wave periods due to the factory sampling frequency of 1.28Hz. The data were sent to IBW PAN with several longer delivery interruptions. Over the period of six years, using this method as many as 170,189 records were collected. Based on the analysis of this data, 31 pairs of significant wave heights and wave periods (H_s , T) which uniformly cover the domain of typical wave conditions were chosen. More details regarding the selection of this wave conditions are described in the Results section, when describing the measurement results. Each element of this set was considered together with 19 discrete wave directions, from NWW to NEE. This means that the total of 547 wave conditions characterized by (H_s , T , dir) were examined as test cases.

The significant wave steepness was calculated based on the height and the period of the significant wave, Eq. (1).

$$\xi = \frac{H_s}{L} = \frac{2\pi H_s}{gT_p^2}. \quad (1)$$

Numerical modelling of nearshore flows

Two spectral numerical wave models: SWAN (Simulating WAVes Nearshore) cycle III (Booij et al., 1996) and XBeach (Roelvink et al., 2010) were used. These complex models simulate the generation of waves by wind and wave propagation, taking into account a number of physical phenomena determining the wave field, such as shoaling, refraction, non-linear interaction between the waves and

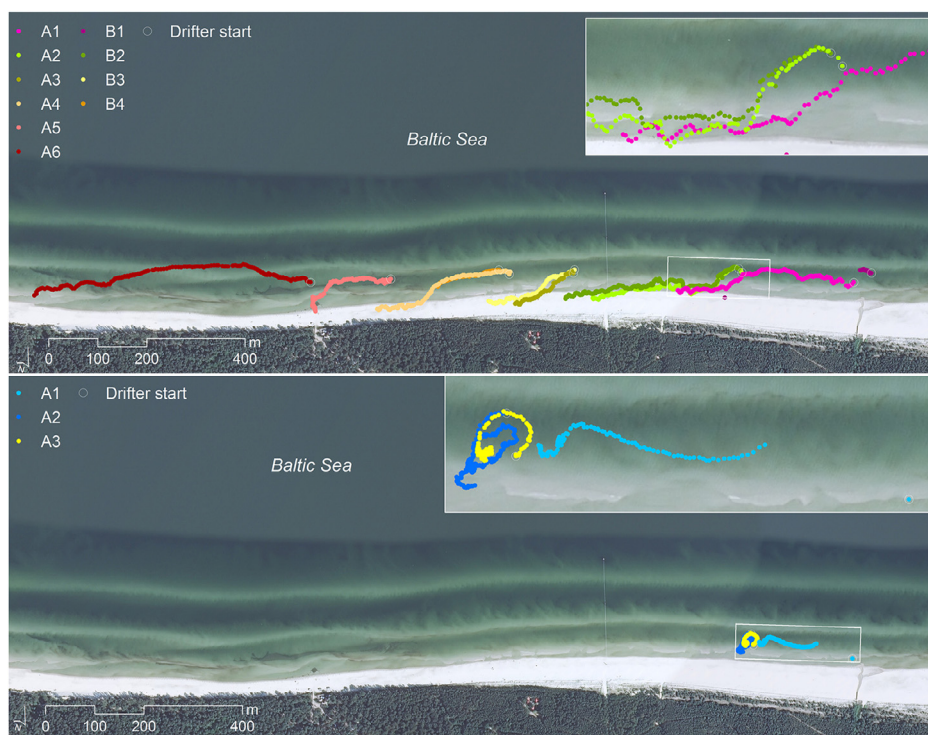


Figure 4 Tracks of drifters measured during field expeditions: 14.01.2016 (the top panel) and 15.04.2016 (the bottom panel). The aerial photo (Head Office of Geodesy and Cartography, retrieved 15.10.2017) is demonstrative and was not done at the same time as measurements, so in some cases the drifters' trajectories end at the beach, which actually didn't happen.

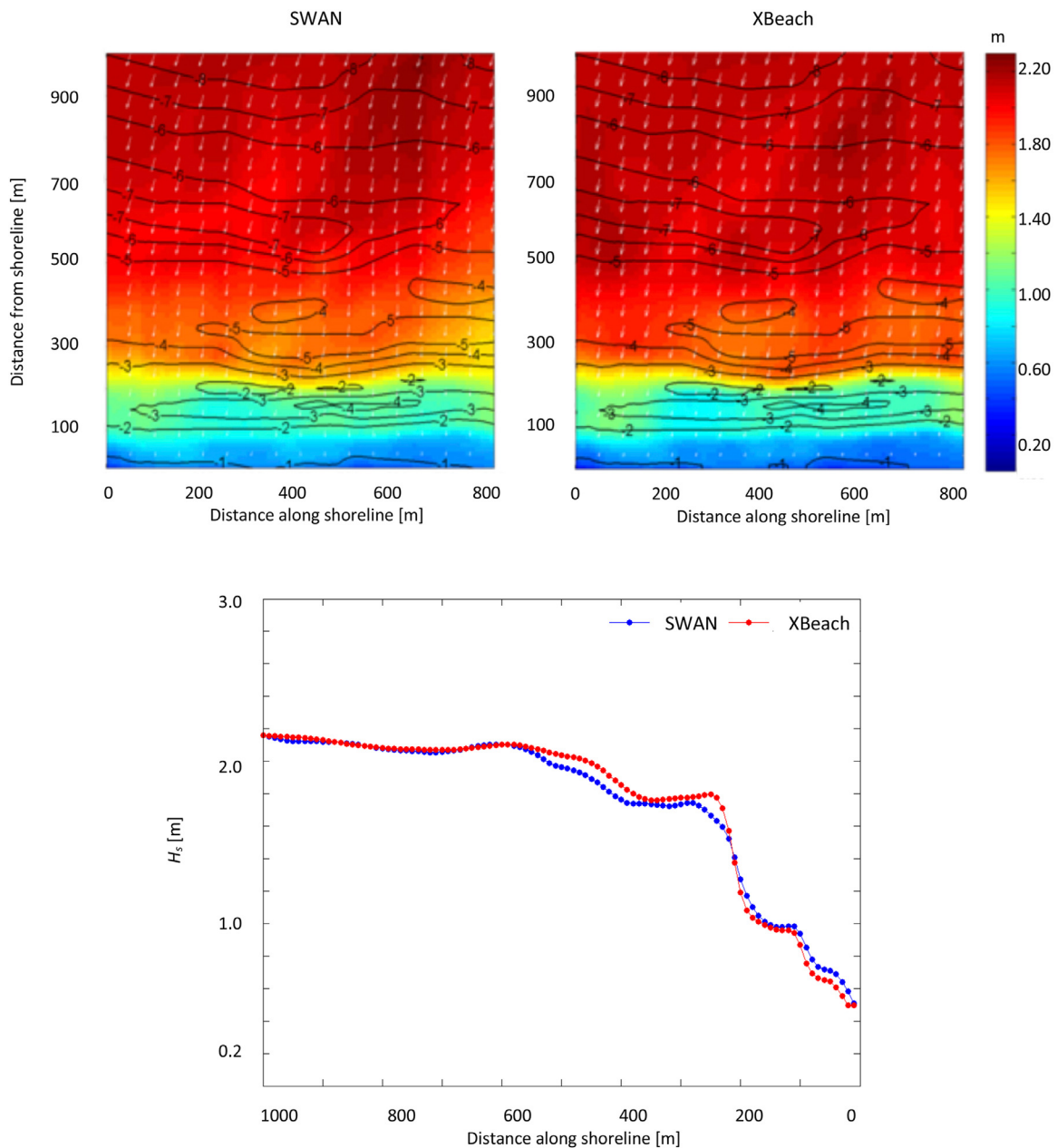


Figure 5 The upper figures: The H_s field modelled by SWAN and XBeach, seaward boundary: $H_s = 2.16$ m, $T = 5.50$ s, $dir = 344^\circ$; the bottom figure: H_s profile along the central transect.

wave energy dissipation. The SWAN model, designed for coastal sea areas, additionally includes energy dissipation by friction at the bottom and refraction due to ocean currents. XBeach, developed to simulate hydrodynamic and morphodynamic processes and impacts on sandy coasts with a domain size of kilometers and on the time scale of storms, takes into account also bottom changes caused by sediment transport. SWAN and XBeach solve the wave action balance equation (for details see e.g. Cieřlikiewicz et al. (2017)).

The SWAN model was used to generate nearshore wind-wave parameters for XBeach model cross-validation. Calculations were done in two steps using numerical meshes presented in Fig. 1:

- The external grid, with spatial resolution of $100 \text{ m} \times 100 \text{ m}$, covering the area between the coastline and a certain location offshore with generalized bathymetric data;
- The internal grid, with spatial resolution of $10 \text{ m} \times 10 \text{ m}$, covering the area up to 1 km offshore, with detailed bathymetric data.

For details, see Grusza (2007). All SWAN parameters were chosen according to the previous extended studies, including the model configuration and results validation in the area of study (Gic-Grusza and Dudkowska, 2014; Reda and Papińska, 2002).

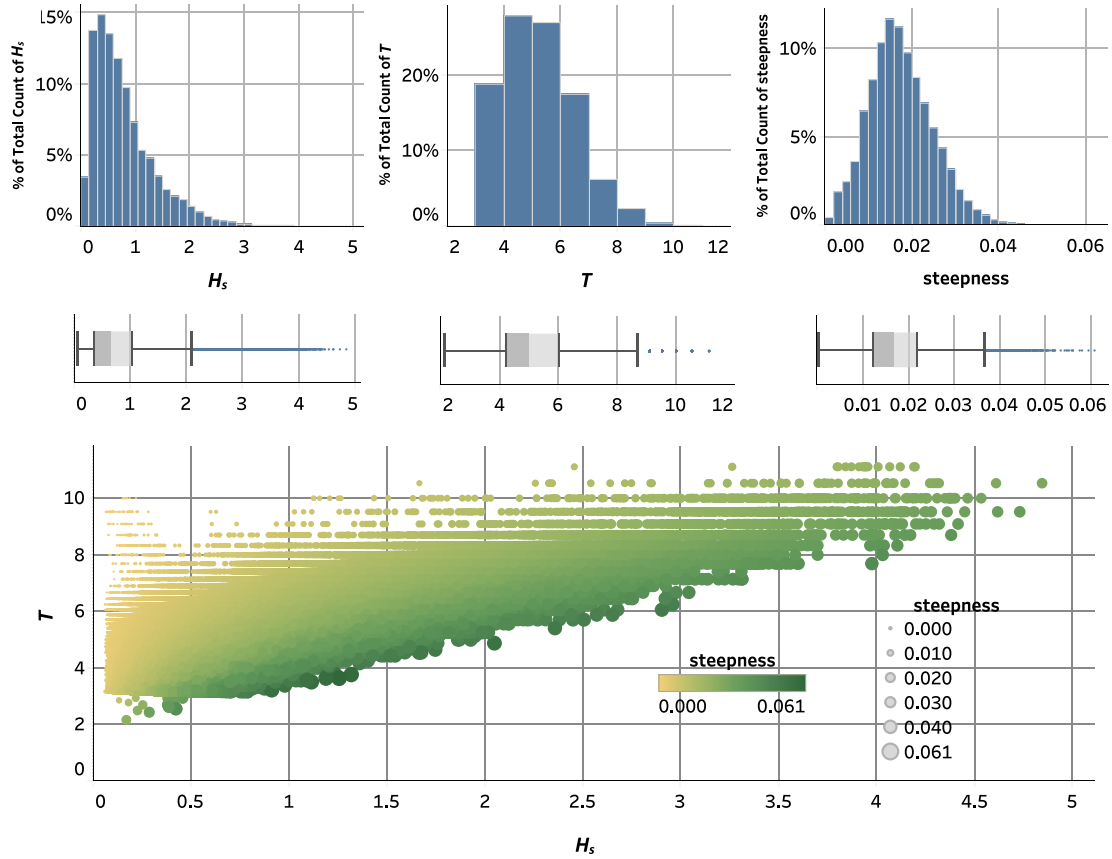


Figure 6 Statistical description of deep water wave conditions in the vicinity of Lubiatowo in years 2013–2018, basing on data from buoy measurements. The upper panel: histograms and box plots of significant wave height, wave period and steepness. Whiskers extend to data within 1.5 times the interquartile range IQR. The bottom panel: scatter plot of significant wave height vs wave period (170,189 points). Wave steepness characteristic for each pair of (H_s, T) is presented as size and colour of marker.

The numerical reconstruction of the coastal flow was performed with the use of XBeach model (Roelvink et al., 2010). The model solves coupled 2D horizontal equations for wave propagation, flow, sediment transport and bottom changes. In this paper sediment transport and bottom changes were not included in calculations. The wave forcing in the shallow water momentum equation is obtained from a time dependent version of the wave action balance equation, Eq. (2).

$$\frac{\partial A}{\partial t} + \frac{\partial c_x A}{\partial x} + \frac{\partial c_y A}{\partial y} + \frac{\partial c_\Theta A}{\partial \Theta} = \frac{D_w}{\sigma}, \quad (2)$$

where A – the wave action, σ – intrinsic wave frequency, Θ – the angle of incidence with respect to x -axis, c_x , c_y , c_Θ – wave action propagation speed in x -, y - and Θ -direction, D_w – total wave dissipation in each directional bin.

Depth-averaged Generalized Lagrangian Mean (GLM) formulation of the shallow water equations are applied to compute the wave induced mass-flux and the return flow (Roelvink et al., 2010). Lagrangian velocity is defined for a water parcel as the average distance traveled during one wave period. The components of Lagrangian velocity: cross-shore u^L and long-shore v^L are related to the components of Eulerian velocity (u^E, v^E) – the fluid velocity at a fixed posi-

tion and to the components of the Stokes drift (u^S, v^S) by:

$$u^L = u^E + u^S \quad v^L = v^E + v^S. \quad (3)$$

The depth-averaged u^L and v^L are obtained from the GLM-momentum and continuity equations in the form of set of equations Eq. (4).

$$\frac{\partial u^L}{\partial t} + u^L \frac{\partial u^L}{\partial x} + v^L \frac{\partial u^L}{\partial y} - f v^L - \nu_h \left(\frac{\partial^2 u^L}{\partial x^2} + \frac{\partial^2 u^L}{\partial y^2} \right)$$

$$= \frac{\tau_{sx}}{\rho h} - \frac{\tau_{bx}^E}{\rho h} - g \frac{\partial \eta}{\partial x} + \frac{F_x}{\rho h},$$

$$\frac{\partial v^L}{\partial t} + u^L \frac{\partial v^L}{\partial x} + v^L \frac{\partial v^L}{\partial y} - f u^L - \nu_h \left(\frac{\partial^2 v^L}{\partial x^2} + \frac{\partial^2 v^L}{\partial y^2} \right)$$

$$= \frac{\tau_{sy}}{\rho h} - \frac{\tau_{by}^E}{\rho h} - g \frac{\partial \eta}{\partial y} + \frac{F_y}{\rho h},$$

$$\frac{\partial \eta}{\partial t} + \frac{\partial h u^L}{\partial x} + \frac{\partial h v^L}{\partial y} = 0, \quad (4)$$

where τ_{bx}, τ_{by} – bottom shear stresses, calculated with the Eulerian velocities, η – the water level, F_x, F_y – the wave induced stresses, ν_h – the horizontal viscosity, f – Coriolis coefficient.

The Lagrangian velocities are used to calculate the wave action propagation speeds according to Eq. (5), which takes

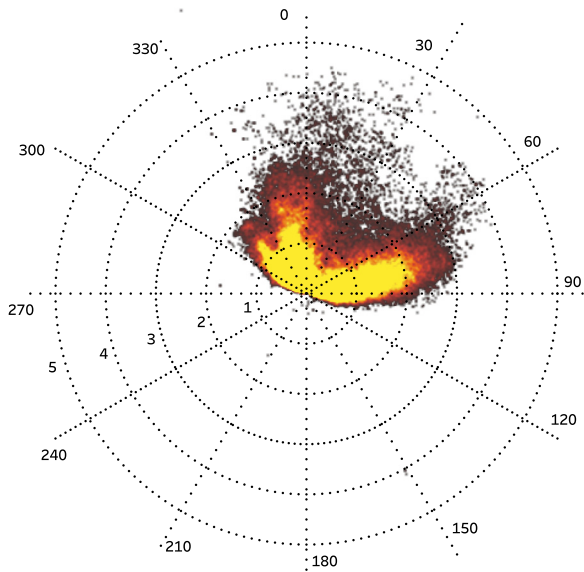


Figure 7 Distribution of wave directions and significant wave height occurring in 2013–2018, basing on data from bouy measurements (170,189 points are shown). Pole system is used – each point of the graph presents the wave direction (angle in the coordinate system) and the significant wave height (distance from the origin). Nautical convention is adopted for wave directions (the direction where the waves are coming from, eg. 270 means that wave is propagating from the west to the east). The colors indicate the frequency of occurrence of wave conditions (H_s, Θ): the yellow points – the most frequent ones, the black points – appearing the least frequently.

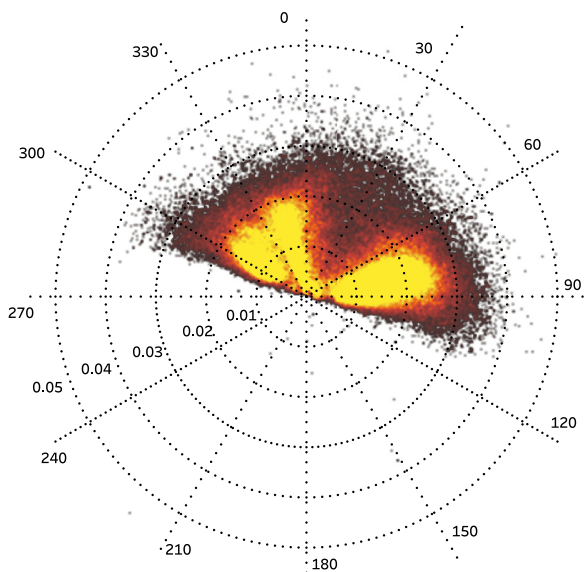


Figure 8 Distribution of wave directions and wave steepness for the data presented in Fig. 7. Each point of the graph presents the wave direction (angle in the pole coordinate system) and the wave steepness (distance from the origin in the pole coordinate system). The colors indicate the frequency of occurrence of wave conditions (ξ, Θ): the yellow points – the most frequent ones, the black points – appearing the least frequently.

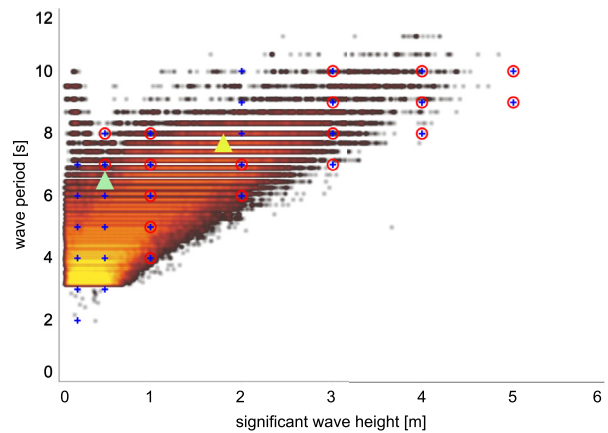


Figure 9 (1) Coloured open circles – distribution of significant wave height and wave period for the data presented in Fig. 7, the colours indicate the frequency of occurrence of wave conditions (H_s, T) analogous to Fig. 7, 170,189 points are shown; (2) blue crosses – 31 test wave conditions (H_s, T) for which coastal flows were examined; (3) red open circles – 18 wave conditions (H_s, T) for which rip currents were modelled; (4) yellow and green triangles – wave conditions during field surveys in CRS Lubiatowo.

into account wave-current interaction.

$$\begin{aligned}
 c_x(x, y, t, \Theta) &= c_g \cos(\Theta) + u^L \\
 c_y(x, y, t, \Theta) &= c_g \sin(\Theta) + v^L \\
 c_\Theta(x, y, t, \Theta) &= \frac{\sigma}{\sinh 2kh} \left(\frac{\partial h}{\partial x} \sin \Theta - \frac{\partial h}{\partial y} \cos \Theta \right) \\
 &\quad + \cos \Theta \left(\sin \Theta \frac{\partial u}{\partial x} - \cos \Theta \frac{\partial u}{\partial y} \right) \\
 &\quad + \sin \Theta \left(\sin \Theta \frac{\partial v}{\partial x} - \cos \Theta \frac{\partial v}{\partial y} \right). \tag{5}
 \end{aligned}$$

XBeach model settings which were applied for the purposes of this paper: (i) neglecting of sediment transport and bottom changes, (ii) wave current interaction option, (iii) stationary wave boundary condition at the seaward boundary, which means that a uniform, constant wave energy distribution is set, based on the given values of wave height and period; Neumann lateral boundaries (iv) the roller model which can give a shoreward shift in a wave-induced setup, return flow and longshore current.

In addition, with the use of drifter option there were examined the details of the flow. Drifters are objects that move with Lagrangian mean velocity, and their positions are evaluated at each time step. During numerical simulations drifters were implemented after 600 s of the model spin-up, and the total run duration was set as 1200 s, which was sufficient for the analysis of drifters' behaviour.

The computational grid used in XBeach model (10 m × 10 m, Fig. 2) was rotated clockwise by 17 degrees relative to the original geographical coordinates of the local system, where the x-axis is parallel to the shore, and the y-axis is perpendicular to the shore (Grusza, 2007). Next, the grid was rotated by 90 degrees in order to adjust it to the XBeach convention, where x-axis is perpendicular to the shore. To overcome the artificial wave breaking

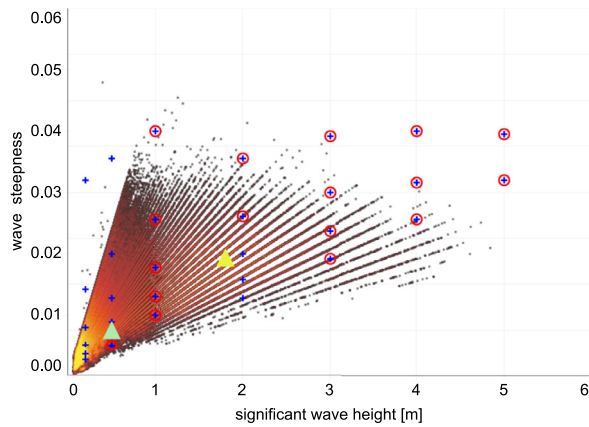


Figure 10 (1) Coloured open circles – distribution of significant wave height and wave steepness for the data presented in Fig. 7, the colours indicate the frequency of occurrence of wave conditions (H_s , ξ) analogous to Fig. 7, 170,189 points are shown; (2) blue crosses – 31 test wave conditions (H_s , ξ) for which coastal flows were examined; (3) red dots – 18 wave conditions (H_s , ξ) for which rip currents were modelled; (4) yellow and green triangles – wave conditions during field surveys in CRS Lubiatowo.

effect on the grid border, the grid was extended to 1400 m in the seaward direction, with uniformly increasing depth up to 20 m. This procedure enabled obtaining the ratio $c_g/c = 0.66$ recommended by XBeach model users on the seaward boundary of the proper computational grid.

The dynamics of water in the model domain is caused by wave coming from the open sea which is defined on seaward open boundary conditions by wave height, period and direction. Among various model output parameters are available fields of significant wave height H_s and vertical

averaged water velocity. Additionally, drifter module allows obtaining trajectories of virtual tracers.

The gap in the bar was artificially introduced into the bathymetry in order to simulate the rip channel. First, the calibration and model validation were conducted by comparison of the modelled wave parameters to the results of SWAN model, which configuration in the study area was discussed in previous studies (Reda and Paplińska, 2002). The second model validation was conducted using the tracks of virtual tracers and their velocities as well as corresponding in situ measured flows. The H_s fields obtained based on XBeach modelling were compared with the H_s field determined by the SWAN model, the results for one chosen wave situation are presented in Fig. 5. The absolute errors of individual H_s values were in the range of 0.08–0.35 m, while the relative errors were in the range of 4%–22%. After model calibration, nearshore wave and currents fields were simulated for all 589 test cases.

4. Results

Deep water waves

The results obtained from the analysis of deep water wave conditions in the vicinity of Lubiatowo in 2014 are presented in Figs. 6–10. Basic statistics are presented as histograms and box plots of significant wave heights H_s , wave period T and resulting wave steepness ξ , Fig. 6. It is visible that in the studied area H_s are typically in the range of about 0.4–1.1 m with the median of about 0.6 m and occasionally occurring waves of height up to 5.0 m. The median of wave period T is 5.0 s, waves of periods between 4.3 and 6.1 s occur most often, the maximal value of T was about 10 s. The most common are waves of steepness in the range 0.012–0.022, with median about 0.017 and

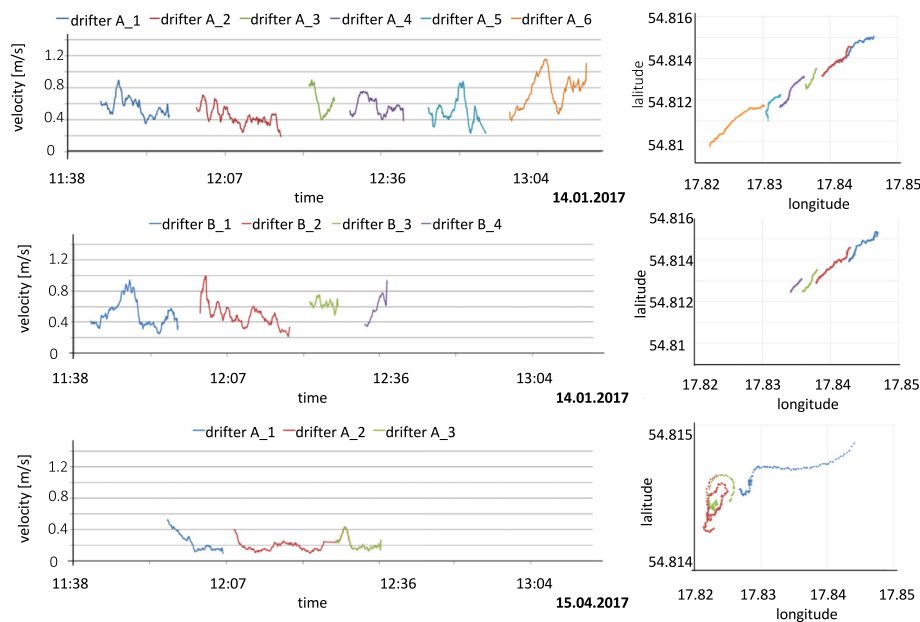


Figure 11 The actual velocities of drifters following their paths presented in Fig. 4 during two expeditions in CRS Lubiatowo.

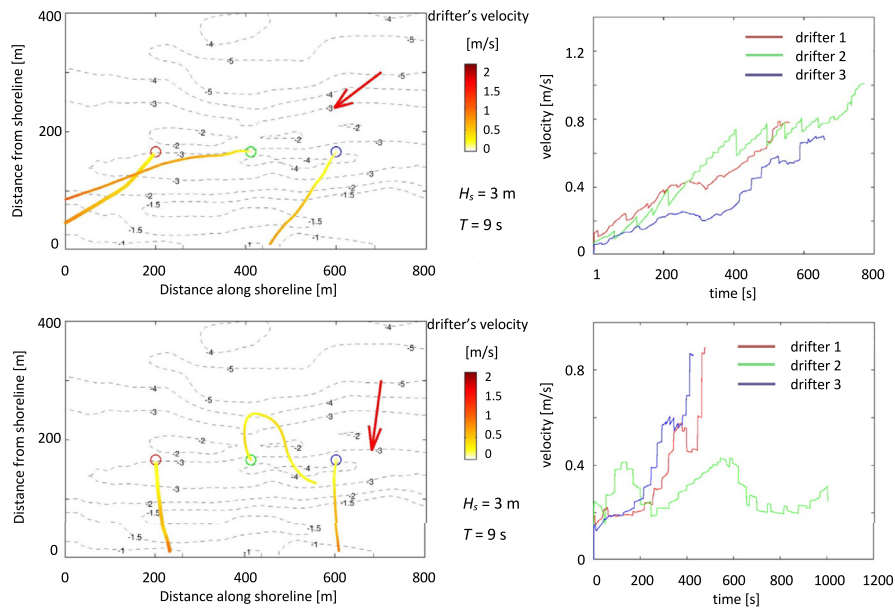


Figure 12 The tracks of virtual drifters obtained by numerical simulation with the use of XBeach model, the simulation time was 1200 s. The red arrow indicates the deep water wave direction, the coloured open circles – the start positions of drifters.

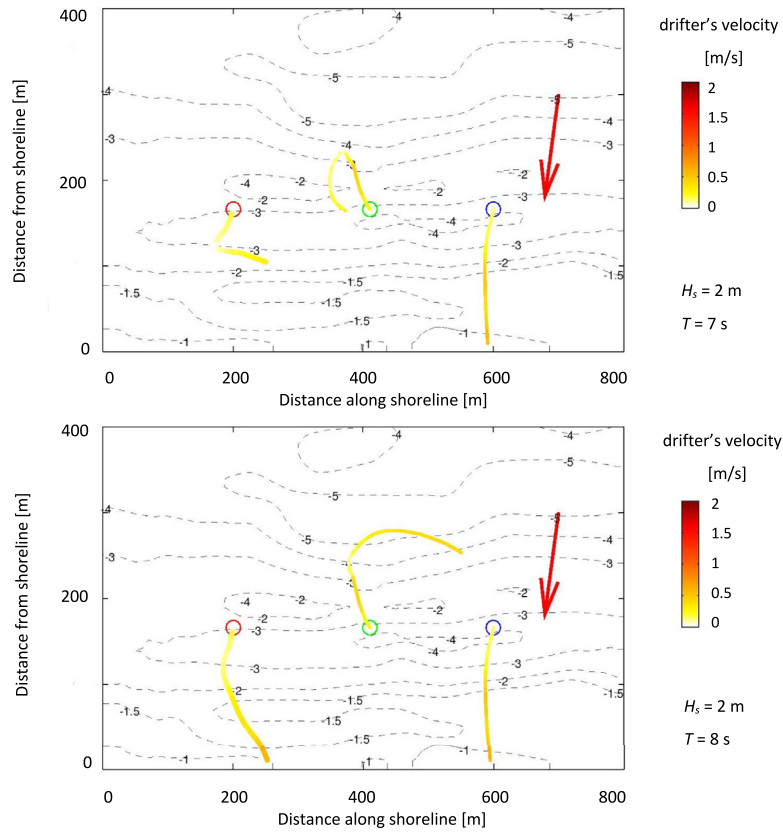


Figure 13 The tracks of virtual drifters (analogous to those shown in Fig. 12). Input wave parameters similar to those prevailing during the expedition in January.

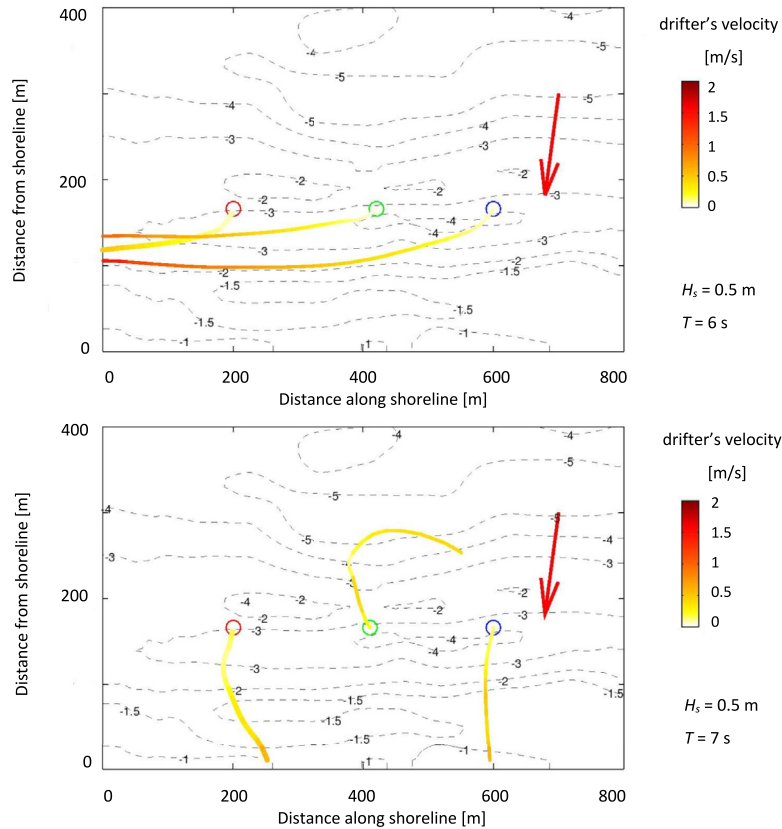


Figure 14 The tracks of virtual drifters (analogous to those shown in Fig. 12), input wave parameters similar to those prevailing during the expedition in April.

maximal value of about 0.06. Such maximal steepness is characteristic of the waves with the lowest periods for the given height, while minimal values are characteristic of the highest periods (Fig. 6), as a direct consequence of Eq. (1).

Offshore waves propagating towards the northern directions are of low heights and occur rarely. Among onshore waves, these propagating towards the west are higher (the most frequent are up to about 2 m) than the waves propagating in the east direction (the most frequent are up to about 1.5 m), Fig. 7. The steepness of onshore waves in typical situations does not exceed the value of 0.04, Fig. 8. Waves with steepness up to about 0.02 are prevailing in the area concerned.

Based on the above analysis, a set of 31 wave conditions given by pairs of H_s and T was selected, which are likely in the studied region. The range and distribution of H_s , T and ξ were taken into account during selection, Figs. 7 and 8.

Lagrangian measurements

Nearshore flows were estimated in situ taking Lagrangian measurements. The routes of the GPS drifters floating freely at the sea surface were tracked during two expeditions. There were six throws of drifter A (the smaller one), four throws of drifter B (the bigger one) on 14.01.2016, and three throws of drifter A on 15.04.2016. The recorded tra-

jectories of drifters are presented in Fig. 4. The wave was higher and steeper during the first expedition in January than during the second one in April. The actual velocities of drifters following their paths along the shoreline are presented in Fig. 11 and the details of the drifters' paths are summarized in Table 3.

It is apparent from the top panel of Fig. 4 that during the first expedition the drifters released at the distance of about 100 m from the shoreline floated along the shore and after several minutes came back to the beach. The trajectory of a drifter does not depend on its size and weight: smaller and bigger drifters thrown close to each other moved along similar routes, and had similar velocities. For example, see throws 1–4 of A and B drifters.

Averaged over the whole route drifters' velocities measured during the first expedition were higher than during the second expedition, see Table 3. The mean velocity of drifters released 10 times on 14.01.2016 was 0.55 m/s with a standard error of 0.03 m/s, and of those released 3 times on 15.04.2016 was 0.23 m/s with a standard error of 0.02 m/s.

The details of the drifters routes, namely their actual velocities and trajectories are presented in Fig. 11. Short-term fluctuations of velocities were smoothed out by a moving average filter with a period of 60 seconds.

Regarding the survey from 14.01.2016, initial velocities of drifters were in the range of about 0.4–0.6 m/s. The

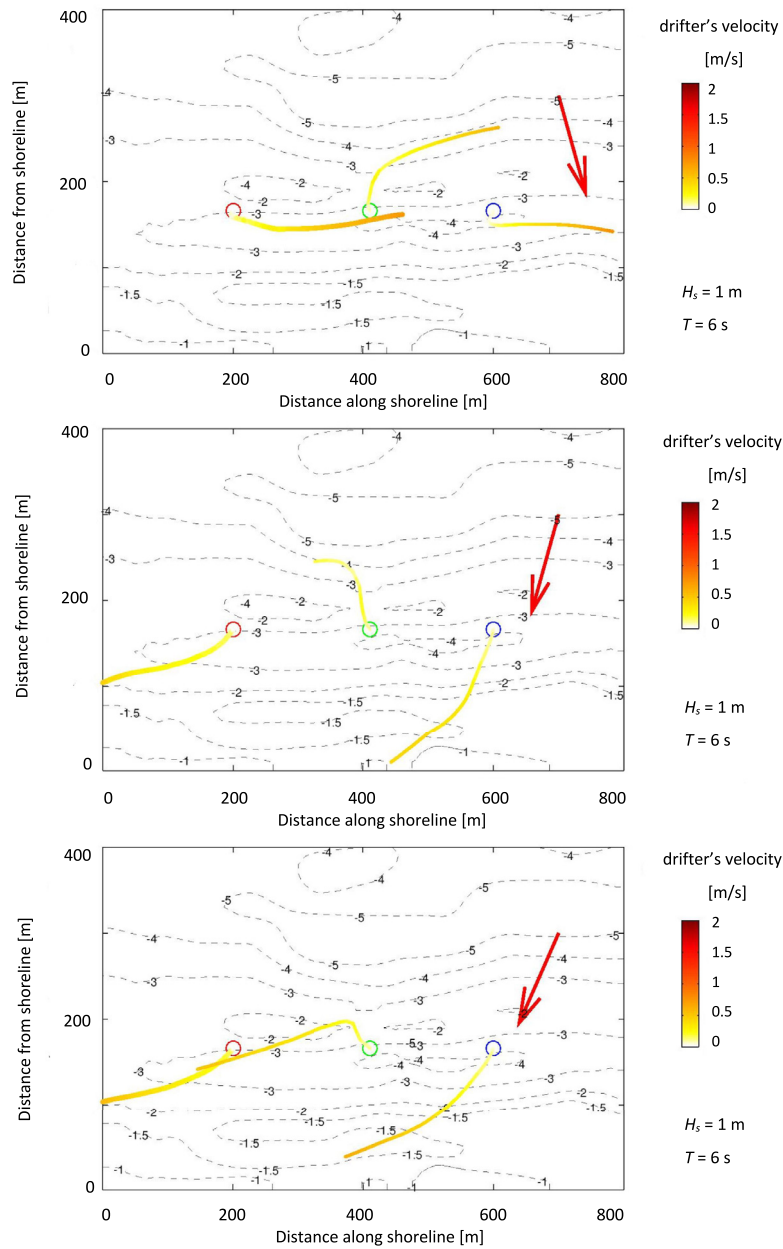


Figure 15 The tracks of virtual drifters (analogous to those shown in Fig. 12), input wave parameters: $H_s = 1$ m, $T = 6$ s, $\xi = 0.018$, $dir: (340, 20, 30)$.

peaks in velocities (up to 1–1.2 m/s) were probably connected to crossing the bar. The changes of the drifters' velocities during their route along the coastline were partly related to the varying depth around bars, but were also caused by an accidental contact with the ground. Thus, a reliable examination of the drifters' velocity changes associated with the nearshore current field in high wave conditions was not possible.

In summary, all the measurements of 14.01.2016 showed a longshore flow typical of this kind of coast, which was quasistationary in the study area (about 1.5 km of coast).

The results of the second expedition (15.04.2016) are the following: the initial velocities of drifters were in the range about 0.2–0.5 m/s, so were smaller than those recorded in January. Also, two trajectories of a drifter observed in April were significantly different from the typical alongshore drifters' routes which were recorded in January. After the first throw, drifter A floated about 250 m for 15 minutes in a typical way, alongshore with the velocity decreasing from about 0.5 to 0.1 m/s. By contrast, after the second throw drifter A moved along the loop about 100 m in diameter. Upon returning to the shore, it was released again and it repeated this loop-shaped route once more.

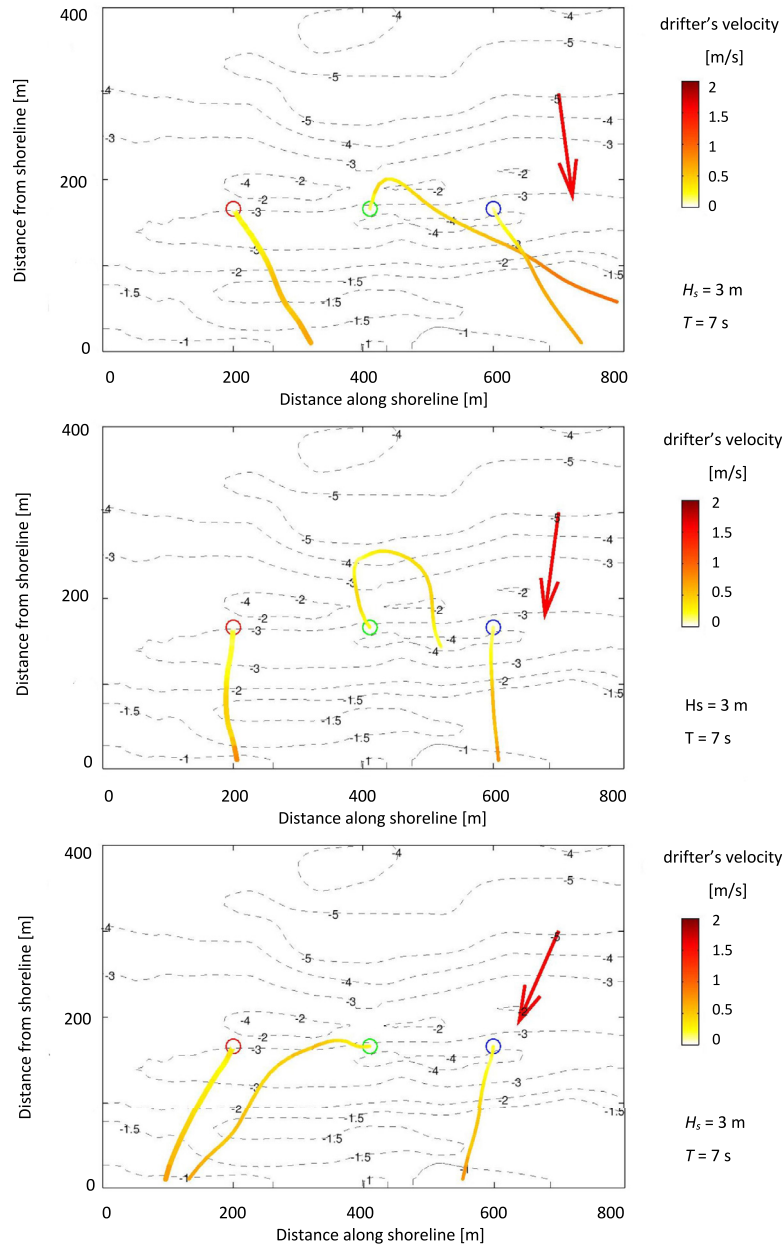


Figure 16 The tracks of virtual drifters (analogous to those shown in Fig. 12), input wave parameters: $H_s = 3$ m, $T = 7$ s, $\xi = 0.039$, $dir: (350, 10, 30)$.

The actual velocities during these untypical flows did not differ from those observed during the first throw, and were about 0.2–0.4 m/s. Taken together, these results provide important insights into two types of nearshore flows.

Modelling approach

In order to confirm hypotheses stated in the Introduction, modelling approach was used. Tracks of virtual tracers were simulated with the use of XBeach model in 589 numerical experiments. The input data for the model are: (1) morphological conditions conducive to rip current generation;

(2) boundary conditions (H_s , T , dir) that represent typical wave fields in the studied area. The set of wave boundary conditions applied in all 589 test cases is presented in Figs. 9, 10, and 18. This set was obtained based on analysis of long term measurements described at the beginning of this section.

There are two subsets of all examined virtual tracers' trajectories. The former contains routes leading directly to the shore with the approach angle dependent on the wave direction to which we refer as regular flows. The latter contains routes with some features typical of rip currents, i.e. offshore flows with increasing velocity. In this paper, we

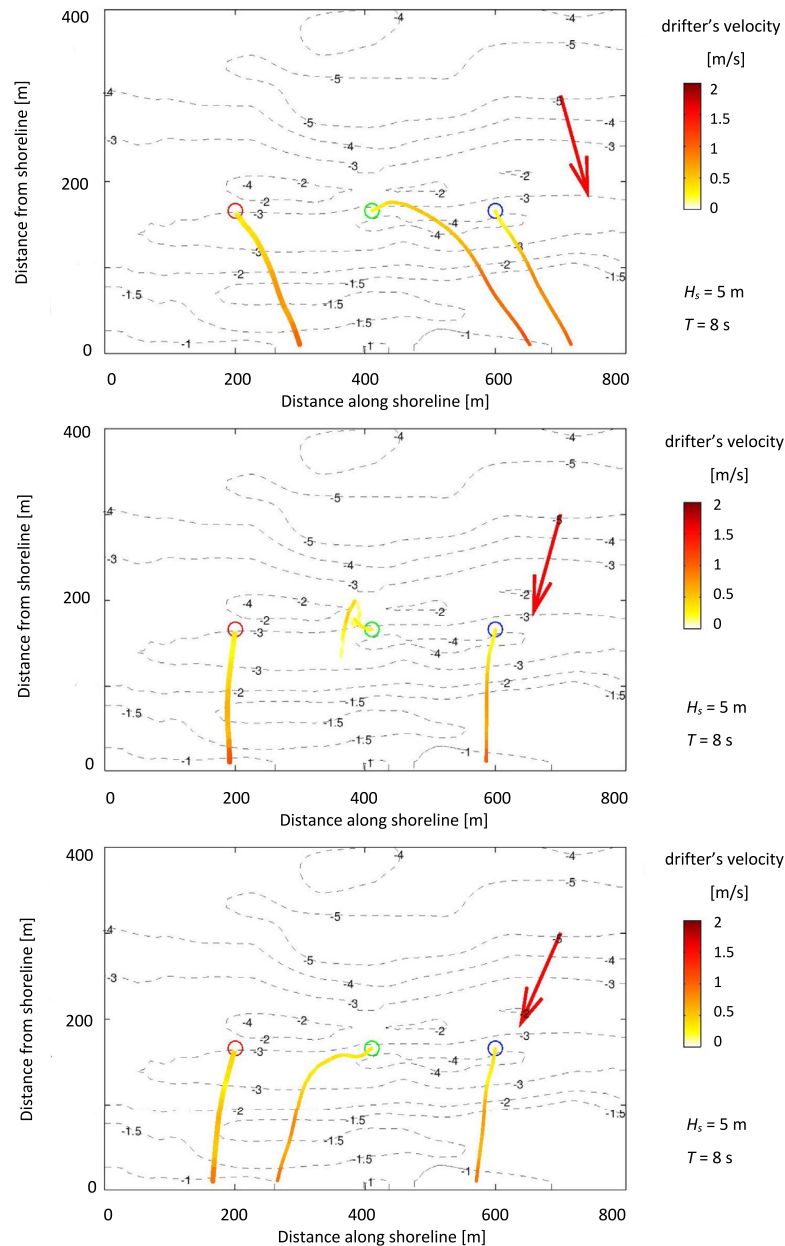


Figure 17 The tracks of virtual drifters (analogous to those shown in Fig. 12), input wave parameters: $H_s = 5$ m, $T = 8$ s, $\xi = 0.05$, $dir: (340, 20, 30)$.

will use the term rip current to describe such type of tracer trajectory. The examples of these two typical flows are presented in Fig. 12, the regular flow in the top panel, and the rip current in the bottom panel. These graphs show that the drifter's velocity changes along its route according to the following rules. In the case of regular flows (all drifters in the top panel and drifter 1 and 3 in the bottom panel) velocity increases as the depth decreases. Occasionally velocity peaks in the areas of rapid change of bathymetry, see for example drifters 1 and 3 during about 300–400 s of simulations. The movement of a rip current type drifter

(drifter 2 in the bottom panel) is characterized by a rapid growth of velocity in the vicinity of rip channel on the way offshore and back along the loop.

Figs. 13 and 14 show results of simulations with wave boundary conditions corresponding to those prevailing during the expeditions in January and in April. A deep sea wave was slightly deviated to the west from onshore direction during both expeditions, while wave steepness were different, about 0.02 during the expedition in January and about 0.01 in April. Virtual tracers' routes in wave conditions similar to those during the first expedition (Fig. 13)

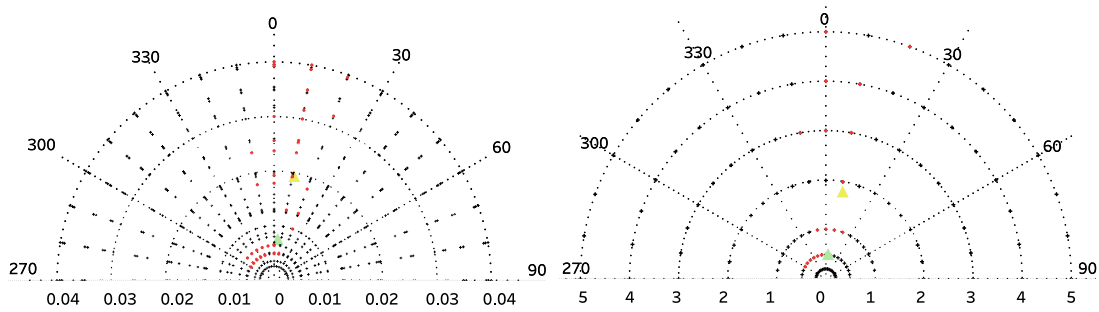


Figure 18 The left diagram: the significant wave steepness with the wave direction (ξ , *dir*). The right diagram: the significant wave height with the wave direction (H_s , *dir*). Pole coordinate system is used in which the angle represents the wave direction, the distance from the origin represents ξ or H_s respectively. Nautical convention is adopted for wave directions (the direction where the waves are coming from, eg. 270 means that wave is propagating from the west to the east). (1) black dots represent $31 \times 19 = 589$ test wave conditions for numerical experiments; (2) red dots – 42 wave conditions for which rip currents were modelled, corresponding to 18 points presented in Fig. 10; (3) triangles – wave conditions during field surveys in Lubiatowo.

Table 3 Drifters' paths characteristics.

	distance [m]	time	average velocity [m/s]
14.01.2016			
A 1	437.5	00:12:50	0.56
A 2	410.4	00:15:45	0.44
A 3	189.4	00:05:10	0.61
A 4	335.4	00:09:50	0.55
A 5	307.4	00:11:07	0.51
A 6	615.4	00:14:10	0.72
B 1	478.4	00:16:40	0.48
B 2	499.9	00:16:55	0.49
B 3	213.5	00:05:40	0.62
B 4	134.7	00:04:20	0.51
15.04.2016			
A 1	243.8	00:15:30	0.26
A 2	333.7	00:27:45	0.20
A 3	115.3	00:08:35	0.22

are of the rip current type. The maximal velocities are up to about 0.6 m/s. It is interesting to note that the direction of rip current 'loop' differs for the wave steepness of 0.03 (counter-clockwise) and 0.02 (clockwise). Simulations for wave conditions similar to those during the second expedition (Fig. 14) are of a regular flow type, with tracers flowing alongshore with increasing velocity.

Figs. 15–17 show exemplary trajectories of drifters for the wave heights of 1, 3, and 5 m and wave directions close to the onshore territory. In these cases an irregular velocity field is more likely to be generated for wave direction closer to normal to the shore.

The total results of all 589 test cases are presented in Fig. 18. It shows that the rip current type of flows were simulated (i) for wave directions in the range from 300 (NW) to 20 (NNE), thus almost normal to the shore; (ii) for all tested wave heights and wave steepness. Among 42 wave conditions for which currents were reproduced there were: the most (18 cases) for wave directions from NNE, 12 cases for wave directions from N, and 12 cases

for wave directions from NW. There is no symmetry in the flow field resulting from corresponding western and eastern wave directions. The rip currents were generated by waves of lower heights ($H_s < 1$) and steepness ($\xi < 0.01$) when approaching from the NNW direction, and by larger (H_s up to 5 m) and steeper (ξ up to 0.04) waves in the other case.

5. Discussion

The wave conditions during both field expeditions were similar in terms of the period and direction of the wave, while the wave heights and the resulting steepnesses were considerably different from each other. The wave directions were almost normal to the shore which, according to theories describing rip currents, are conducive to their formation. Moreover, the wave periods were above the mean value in the studied area. In the case of waves with long periods (long waves), most of the energy reaches the shore and waves break down near the shoreline. The dissipated wave energy is transformed into energy of such phenomena as: turbulence, reflected waves and currents of wave origin. In the case of oblique wave direction longshore current is generated, which has a dominant role in the studied area. In the case of shore-normal waves, a return or rip current is generated.

The example of a rip current was registered in Lagrangian measurements during the second day of measurements. On this day a wave period was slightly shorter than during the first expedition, but with the steepness being about two times lower. It means that during the second expedition the waves dissipated much closer to the shore, thus more wave energy was transported into the close vicinity of the shoreline. That was probably the reason why, under favourable morphological conditions (local lowering of the bar), the onshore stream of water generated close to the shore could not be compensated by the return current, and a more intense rip current was generated.

However, it is not possible to draw conclusions about the prevalence of occurrence of rip currents on the basis of one observation. Admittedly, at the time when a rip current was observed, the wave height, period and steepness were similar to the most typical ones in the studied area, Figs. 9 and

10. But the wave moved from the NE direction, which is not most common (the predominant waves come from NWW directions), Figs. 7 and 8. Therefore it cannot be said that these were the most frequent wave conditions. Given the relatively narrow area of research and a small number of tests, this observation may suggest the universality of rip currents in the studied area. On the other hand, it should be noted that according to the theory, a wave direction almost normal to the shore is favourable for the appearance of rip current. All these arguments suggest that due to the difficulty of estimating the frequency of rip currents occurrence, model studies are necessary.

In order to test the occurrence of rips in a wide range of wave conditions, numerical simulations have been conducted. It appeared that nearshore flows with typical rip currents features occurred in 42 of the 589 test cases, which is about 7% of the analysed wave situations.

The simulations demonstrated that rip currents emerge only for a restricted range of wave directions, i.e. wave approaching from the north, almost perpendicularly to the shore. However, not all wave conditions with favorable wave direction generated rip currents. Simulations did not indicate similar limitations for the wave height or steepness, but, there are some combinations of H_s and T for which currents are not generated. In summary, the only rule that can be specified based on the modelling results is the one associated with the wave direction. Both the observed lack of symmetry due to the east and west wave direction as well as the occurrence of rip currents during certain specific wave conditions may indicate that there is another important factor influencing the formation of rip currents. We assume that it is local bottom topography. It should be mentioned however that there is no significant difference in the volume of water on the left and right of the basin. Waves that are symmetric with respect to shore normal direction propagate asymmetrically and after reaching the shore give asymmetrical results. Therefore, it is advisable to carry out further model tests examining the impact of bathymetry changes, as well as local wind field on the results to determine the causes of asymmetry in the results.

It is interesting that in the numerical experiment with wave conditions corresponding to in situ measurements from January, a rip current was generated which was not observed in situ. It was probably due to the lack of favourable morphological conditions at the bottom – the rip channel did not form in the measured area.

6. Conclusions

The presented numerical simulations confirmed that bathymetry controlled rip currents in the barred coastal zone can emerge during the wave propagating in the almost shore-normal direction (for wave directions in the range from 300 (NW) to 20 (NNE)). According to the model results, there is no restriction as to the wave height and steepness. However, this study is unable to encompass the entire dynamics of nearshore flow due to limitations of 2D XBeach model.

The typical hydrodynamical situation conducive to rip currents is when large masses of water transported towards

the shore by breaking waves are unable to return towards the open sea in the form of a bottom return current. In this case, in favourable locations (e.g. the local break in the bar), a strong stream of water is created uniformly throughout the water column. Thus, a reliable simulation of a rip current is possible with a correct modelling of the return current. Although there is a mechanism of a return current implemented in the XBeach model, it seems that 3D models address this phenomenon better. Thus, more detailed numerical simulations with the use of 3D flow models should be performed, mainly in order to verify the most controversial results, i.e. rip currents occurring in the presence of a wave with a high steepness.

The mechanism of the rip current initiation considered in this work (the initial disturbance of bathymetry) is only one of the possible scenarios. Nevertheless, the results presented indicate that this phenomenon is rare. In addition, the velocities of both measured and modelled rip currents (up to 0.4 m/s) are small comparing to the velocity of longshore current (up to 1.6 m/s, (Ostrowski et al., 2016)), which occurs when waves approach the shore obliquely. Concluding, the dominant factor affecting the reconstruction of the bottom is longshore current. Rip currents are not very common and have low speeds, so they are not a significant factor in the morphodynamic processes.

Determining the conditions under which rip currents may occur is very important for the investigation of the impact of these flows on the seabed reconstruction, and for the safety of bathers. It is difficult to predict the place and time of their appearance, because it depends on dynamically changing local bathymetry.

This work is one of few attempts to exploring the possibility of the appearance of rip currents in the coastal zone of the South Baltic and provides a background for further research on the issue. Primarily, different flow patterns observed during the two Lagrangian experiments may be explained not only by incident wave conditions, but also by other factors.

In order to verify the assumption about the triggering factor of observed irregular flows, during further research more Lagrangian data should be collected simultaneously with morphology data. Although measurements of bottom topography during an intense wave is difficult, it seems to be crucial to properly understand the hydrodynamic and morphological control over rip currents dynamics along the studied coast. As this location is a representative example of multi-barred coast, presented results are also useful for describing the non-tidal mechanism of rip currents formation on similar beaches.

7. Data Availability

The research data required to reproduce the work reported in Manuscript are available at: <https://bit.ly/2CllePv>.

Acknowledgement

This study was supported by the Institute of Hydro-Engineering of Polish Academy of Sciences (IBW PAN)

by providing multi-annual measurement data and the organization of field research.

References

- Booij, N., Holthuijsen, L.H., Ris, R.C., 1996. The SWAN wave model for shallow water. In: *Proceedings of the 25th International Conference on Coastal Engineering, Orlando, USA*, 1, 668–676.
- Bruneau, N., Bonneton, P., Castelle, B., Pedreros, R., 2011. Modeling rip current circulations and vorticity in a high-energy mesotidal-macrotidal environment. *J. Geophys. Res.* 116(C7), 17, C07026, <https://doi.org/10.1029/2010JC006693>.
- Castelle, B., Almar, R., Dorel, M., Lefebvre, J.-P., Senechal, N., Anthony, E., Laibi, R., Chuchla, R., du Penhoat, Y., 2014. Rip currents and circulation on a high-energy low-tide-terraced beach (Grand Popo, Benin, West Africa). *J. Coastal. Res.* 70, 633–638, <https://doi.org/10.2112/SI70-107.1>.
- Castelle, B., Scott, T., Brander, R., McCarroll, R., 2016. Rip current types, circulation and hazard. *Earth-Sci. Rev.* 163, 1–21, <https://doi.org/10.1016/2016.09.008>.
- Cieślakiewicz, W., Dudkowska, A., Gic-Grusza, G., Jędrasik, J., 2017. Extreme bottom velocities induced by wind wave and currents in the Gulf of Gdańsk. *Ocean Dynam.* 67(11), 1461–1480, <https://doi.org/10.1007/s10236-017-1098-4>.
- Floc'h, F., Mabilia, G.R., Almar, R., Castelle, B., Hall, N., Du Penhoat, Y., Scott, T., Delacourt, C., 2018. Flash rip statistics from video images. *J. Coastal. Res.* 81, 100–106, <https://doi.org/10.2112/SI81-013.1>.
- Furmańczyk, K., 1994. Strefa brzegowa Półwyspu Helskiego w świetle kompleksowej interpretacji zdjęć lotniczych i satelitarnych. *Mar. Sci.* 134(2), 61–80.
- Furmańczyk, K., Andrzejewski, P., Benedyczak, R., Bugajny, N., Cieszyński, L., Dudzińska-Nowak, J., Giza, A., Paprotny, D., Terefenko, P., Zawisłak, T., 2014. Recording of selected effects and hazards caused by current and expected storm events in the Baltic Sea coastal zone. *J. Coastal. Res.* 70, 338–342, <https://doi.org/10.2112/SI70-057.1>.
- Garnier, R., Calvete, D., Falqués, A., Dodd, N., 2008. Modelling the formation and the long-term behavior of rip channel systems from the deformation of a longshore bar. *J. Geophys. Res. Oceans* 113 (C7), art. no. C07053, 18 pp., <https://doi.org/10.1029/2007JC004632>.
- Gic-Grusza, G., Dudkowska, A., 2014. Modeling of wind wave induced sediment transport in the coastal zone of polish marine areas (southern baltic). *Baltic International Symposium (BALTIC), 2014 IEEE/OES: Measuring and modeling of multi-scale interactions in the marine environment*, May 26–29, 2014, Tallinn, Estonia IEEE/OES, 1–5, <https://doi.org/10.1109/BALTIC.2014.6887860>.
- Grusza, G., 2007. Three-dimensional modelling of wave-generated currents in coastal zone. Ph.D. thesis, Inst. Oceanogr., Univ. Gdańsk, Gdynia, Poland, (in Polish).
- Johnson, D., Pattiaratchi, C., 2004. Transient rip currents and nearshore circulation on a swell-dominated beach. *J. Geophys. Res. Oceans* 109, art. no. C020261, 20 pp., <https://doi.org/10.1029/2003jc001798>.
- Johnson, D., Pattiaratchi, C., 2006. Boussinesq modelling of transient rip currents. *Coast. Eng.* 53, 419–439, <https://doi.org/10.1016/j.coastaleng.2005.11.005>.
- Kirby, J., 2017. Recent advances in nearshore wave, circulation and sediment transport modeling. *J. Mar. Res.* 75(3), 263–300, <https://doi.org/10.1357/002224017821836824>.
- Longuet-Higgins, M., Stewart, R., 1964. Radiation stresses in water waves; a physical discussion, with applications. *Deep-Sea Res. Oceanogr. Abstr.* 11 (4), 529–562, [https://doi.org/10.1016/0011-7471\(64\)90001-4](https://doi.org/10.1016/0011-7471(64)90001-4).
- MacMahan, J., Thornton, E., Reniers, A., 2006. Rip current review. *Coast. Eng.* 53, 191–208, <https://doi.org/10.1016/j.coastaleng.2005.10.009>.
- MacMahan, J.H., Thornton, E.B., Stanton, T.P., Reniers, A.J., 2005. RIPEX: observations of a rip current system. *Mar. Geol.* 218 (1), 113–134, <https://doi.org/10.1016/j.margeo.2005.03.019>.
- Ostrowski, R., Schönhofer, J., Szymkiewicz, P., 2016. South baltic representative coastal field surveys, including monitoring at the Coastal Research Station in Lubiatowo, Poland. *J. Marine Syst.* 162, 89–97, <https://doi.org/10.1016/j.jmarsys.2015.10.006>.
- Peregrine, D., 1998. Surf zone currents. *Theor. Comp. Fluid Dyn.* 10, 295–309, <https://doi.org/10.1007/s001620050065>.
- Pitman, S., Gallop, S.L., Haigh, I.D., Masselink, G., Ranasinghe, R., 2016. Wave breaking patterns control rip current flow regimes and surfzone retention. *Mar. Geol.* 382, 176–190, <https://doi.org/10.1016/j.margeo.2016.10.016>.
- Pruszk, Z., Szymkiewicz, P., Ostrowski, R., Skaja, M., Szymkiewicz, M., 2008. Shallow-water wave energy dissipation in a multi-bar coastal zone. *Oceanologia* 50(1), 43–58.
- Reda, A., Paplińska, B., 2002. Application of numerical wave model SWAN for wave spectrum transformation. *Oceanol. St.* 31(1–2), 5–21.
- Roelvink, D., Reniers, A., van Dongeren, A., van Thiel de Vries, J., Lescinski, J., McCall, R., 2010. XBeach Model Description and Manual. Rep.. Unesco-IHE Institute for Water Education, Delft and Delft University of Technology, Delft, Netherlands.
- Rudowski, S., 1970. Smallscale ripples in offshore of the Southern Baltic Sea. *Acta Geol. Pol.* 20(3), 451–483.
- Sabet, B.S., Barani, G., 2011. Field investigation of rip currents along the southern coast of the Caspian Sea. *Sci. Iran.* 18 (4), 878–884, <https://doi.org/10.1016/j.scient.2011.07.017>.
- Schönhofer, J., 2014. Rip currents at beach with multiple bars theoretical description and in-situ observations. Ph.D. thesis, Inst. Hydro-Eng. PAN Gdańsk, Poland, (in Polish).
- Semiring, L., van Dongeren, A., Winter, G., Ormond, M., Briere, C., Roelvink, D.J., 2014. Nearshore bathymetry from video and the application to rip current predictions for the Dutch Coast. *J. Coastal. Res.* 70, 354–359, <https://doi.org/10.2112/SI70-060.1>.
- Short, A.D., Aagaard, T., 1993. Single and multi-bar beach change models. *J. Coastal. Res.* SI 15, 141–157.
- Winter, G., van Dongeren, A., de Schipper, M., van Thiel de Vries, J., 2014. Rip currents under obliquely incident wind waves and tidal longshore currents. *Coast. Eng.* 89, 106–119, <https://doi.org/10.1016/j.coastaleng.2014.04.001>.
- Xie, M., 2012. Three-dimensional numerical modelling of the wave-induced rip currents under irregular bathymetry. *J. Hydrodyn. Ser. B.* 24 (6), 864–872, [https://doi.org/10.1016/S1001-6058\(11\)60314-4](https://doi.org/10.1016/S1001-6058(11)60314-4).